AUTOMATED MEASUREMENT OF ARTERIAL INPUT FUNCTION IN FIRST-PASS MYOCARDIAL PERFUSION MAGNETIC RESONANCE IMAGES USING INDEPENDENT COMPONENT ANALYSIS

Matthew Jacobs[1,2], Mikhail Gorbachev[1,2], Mitchel Benovoy[1,3], Lin-Ching Chang[2], Andrew E. Arai[1], Li-Yueh Hsu[1]

[1]National Heart Lung and Blood Institute, National Institutes of Health, Bethesda, MD, USA
[2]Dept. of Electrical Engineering and Computer Science, Catholic University of America, Washington DC, USA
[3]Ecole Polytechnique de Montreal, Montreal, Canada

ABSTRACT

Quantitative assessment of first-pass cardiac magnetic resonance (CMR) perfusion imaging is useful for detecting coronary artery disease, but it requires the measurement of the arterial input function (AIF) from the left ventricle. This is usually done manually, which is time consuming and subjective. This study presents an automated method for measuring the AIF from the first-pass CMR perfusion images. It was tested on 194 clinical perfusion studies and compared with manual reference measurements. Our results show the proposed method successfully measured 98.79% of the perfusion series, with manual and automated measurements strongly correlating. Temporal statistics were similar for both measurements, showing agreement between the automated and manual AIFs. The automated method, however, more accurately selected the brightest left ventricle pixels and excluded papillary muscles. These improvements may help make AIF measurement and quantitative CMR myocardial perfusion analysis more accurate and readily available.

Index Terms— cardiovascular magnetic resonance, myocardial perfusion imaging, arterial input function

1. INTRODUCTION

First-pass contrast-enhanced myocardial perfusion magnetic resonance imaging (MRI) is a useful diagnostic tool for the detection of coronary artery disease [1, 2]. Quantitative assessment of myocardial contrast dynamics and myocardial blood flow (MBF) provides an accurate evaluation of the myocardial ischemia which appears promising for identifying coronary artery stenosis [3]. However, quantitative assessment of MBF requires the measurement of the arterial input function (AIF), which represents the delivery of contrast to the heart [4]. Such AIFs are typically measured by manually drawing a region of interest (ROI) within the left ventricle (LV) blood pool on a range of 45 to 90 perfusion images. These ROIs must be adjusted for any motion artifacts to obtain the mean time signal intensity (SI) curve. This manual process is time consuming, subject to user variation, and may hinder quantitative assessment of large datasets.

Little research has been performed on automated AIF measurement from CMR perfusion images. In our previous work [5], an automated method was presented to extract the LV blood cavity signal from low-resolution AIF image series by identifying and masking the LV and right ventricle (RV) via radial signal intensity profiling of the difference images. The results were mostly successful, but some cases suffered from incorrect LV masking.

Additional automated AIF detection research has been performed on cerebral perfusion MRI. Carroll et al. [6] presented a method to measure the AIF by excluding late contrast arrival voxels and then selecting the single voxel showing largest signal intensity change. Peruzzo et al.'s [7] method discards voxels poorly fitting expected AIF characteristics and then classifies the remaining voxels with agglomerative hierarchical clustering to select the AIF voxels. Yin et al. [8, 9] also presented two studies, one using the hierarchical clustering and another using a normalized cut clustering scheme to select the final AIF cluster.

This study presents an automated system for measuring the AIF based on time signal intensity changes of the LV cavity from first-pass dynamic contrast-enhanced CMR images to assist quantitative analysis of myocardial perfusion. It is validated on a large dataset consisting of both conventional myocardial perfusion images and low-resolution dedicated AIF images [10]. We show the automated approach is more robust, reproducible, and faster compared to the manual reference measurements.

2. METHODS

2.1. Image Acquisition

A retrospective dataset consisting of 194 clinical CMR perfusion studies was analyzed. All studies contained at least one perfusion imaging at rest, and 160 studies also included pharmacologically-induced stress, totaling 371

imaging series. Gadolinium-enhanced CMR perfusion imaging was performed on a 1.5T Siemens scanner with a saturation recovery steady-state free precession dual-sequence technique [10] at every RR interval over 60 heart beats. For each perfusion imaging, a low-resolution dedicated AIF image series (acquisition and image matrix = 64×48) was acquired for quantitative perfusion analysis in addition to standard myocardial image series (acquisition matrix = 128×80 and image matrix = 256×192) acquired for diagnostic interpretation. An example of each is shown in Figure-1. The low spatial resolution images were specifically designed to maintain the linearity of the LV signal intensity and avoid AIF distortion for quantitative perfusion. The standard resolution images were optimized for measurements of perfusion in the myocardium. At the start of each perfusion acquisition, two proton density (PD) weighted images were also acquired for surface coil intensity normalization.

2.2. Image Processing Algorithm

2.2.1. Motion Correction

Displacement of the heart can occur during image acquisition due to the patient's cardiac or respiratory motion [11]. A non-rigid body image registration technique is applied to correct for motion artifacts that may exist in the image series [12]. This method is based on optical flow computation for non-rigid motion estimation and correction [13]. It is applied to both low-resolution AIF and standard myocardial perfusion image series before subsequent image processing.

2.2.2. Bounding Box Detection

The next step is to locate the heart and candidate ventricle regions in the perfusion series. Candidate regions are identified by thresholding a standard deviation map computed from the time series images. After the binarization, regions that do not match the shape profile or temporal signal characteristics of the ventricles are identified and removed. This includes regions that are highly elongated, have minimal intensity change, or whose peak intensity occur at the very beginning or near the end of the time series. Next, a linear voting scheme is used to determine which two regions are most characteristic of the RV and LV cavities in the images. Features used for voting classification include: distance to the center, distance to other regions, size of each region, SI upslope, peak value (PV), time to peak (TTP), full width at half maximum (FWHM), and an M-value [9] which combines the previous three features as shown in Equation-1.

$$M = \frac{PV}{(TTP * FWHM)} \qquad (1)$$

Potential ventricular regions are characterized by large values of region size, PV, upslope, M-value, small values of TTP and FWHM, and small distances to image center and other regions. Contrast onset time for TTP and upslope calculation is estimated automatically by fitting a straight line between the rising half maximum and peak points backward in time. The intersection of the baseline SI curve and the upslope line is used as the point of contrast onset or arrival time. The selected regions are used to create a bounding box around the heart for time signal detection.

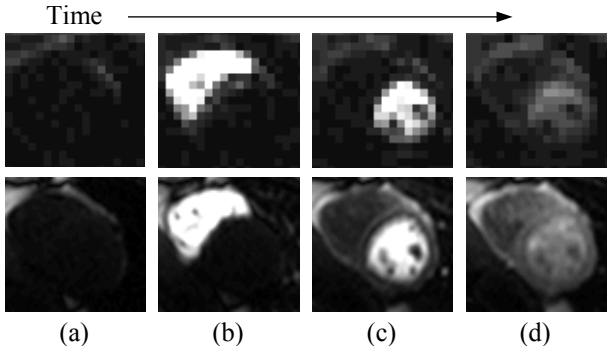

Figure-1. Dynamic contrast enhancement in a low-resolution AIF (top) and a standard (bottom) CMR perfusion image series. Images show (a) baseline, (b) RV, (c) LV, and (d) myocardial enhancement.

2.2.3. Intensity Correction

Signal inhomogeneity exists in CMR images due to surface coil sensitivity profile. An automated version of a surface coil intensity correction (SCIC) algorithm [14] is applied to rectified such inhomogeneity. This method estimates a polynomial signal intensity surface profile from the PD images based on a hierarchical weighting scheme. This estimated intensity surface is used to improve the field homogeneity in the perfusion image series by rescaling the signal intensity. After SCIC, the image series is further adjusted to remove baseline intensity using the maximal intensity projection of pre-contrast perfusion images.

2.2.4. Ventricular Pixel Detection

In order to detect ventricular blood pool pixels in the images, an independent component analysis (ICA) algorithm [15] is used to obtain representative time SI curves from the previously identified bounding box. Assuming a mixture of two primary sources of signal, i.e. the RV and LV, for all pixels in the bounding box, ICA separates and extracts two unique time signals to represent the dynamic contrast of the two ventricles.

Next, all pixels in the bounding box are classified to the RV, LV or background regions by computing their cross correlation to the RV and LV time signals. Pixels with a cross correlation greater than 0.7 are assigned to the matching ventricle, otherwise they are classified to the background region. The RV is identified as being the first region to reach peak intensity, which is then followed by the LV region (see Figure-2).

2.2.5. AIF Extraction

The final step of the algorithm is to select LV pixels that are brighter than a default threshold to compute an average intensity value for each image. This step excludes papillary muscle pixels that may have been included in the LV region from the previous steps; this closely replicates manual analysis, where only a small bright portion of the LV cavity is selected to avoid papillary muscle inclusion. The default threshold was computed from the maximal intensity projection image of the LV region as one standard deviation above the mean value.

2.3. Validation

The performance of the proposed automated method was evaluated on 371 pairs of low-resolution AIF and standard myocardial image series for a total of 742 series. The results of the automated AIF detection were compared to a reference standard created by manually drawing an ROI in the LV blood cavity throughout the entire image series. The resulting automated and manual AIF curves were compared using Pearson's correlation coefficient and normalized root mean square error (RMSE). Other statistics of the AIF were also compared, including TTP, FWHM, PV, SI upslope, and M-value (see section 2.2.2). Accurate AIFs are normally characterized by high values of PV, upslope, M-value, and low values of TTP and FWHM [9]. The execution time of the automated algorithm was also measured on a dataset of 40 image series using an Intel Core i7-3770 3.4GHz CPU and compared against the time required to manually selected ROI for the AIF measurement. Finally, a non-parametric Mann-Whitney U test was used to determine if there were significant differences between the automated and manual AIF measurements.

3. RESULTS AND DISCUSSION

Figure-2 shows examples of automatically detected LV and RV regions from the ICA process and their respective time SI curves. Figure-3 shows the AIF computed from the automatically detected LV pixels versus the manually selected ROI. The correlation coefficient between the manual and automated AIFs averaged 0.996±0.002 over all series. RMSE averaged only 7.83% over the whole series.

Table-1 summarizes the statistical comparison of the automated and manual AIF results from the low resolution

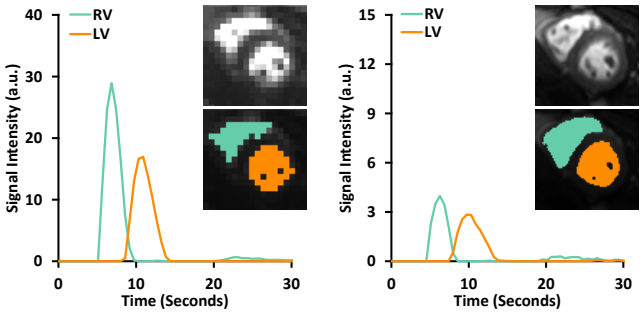

Figure-2. ICA detected RV and LV regions and their respective time-signal intensity curves from a low-resolution AIF (left) and a standard myocardial (right) series. The series maximal intensity projection image is displayed above the mask image for reference.

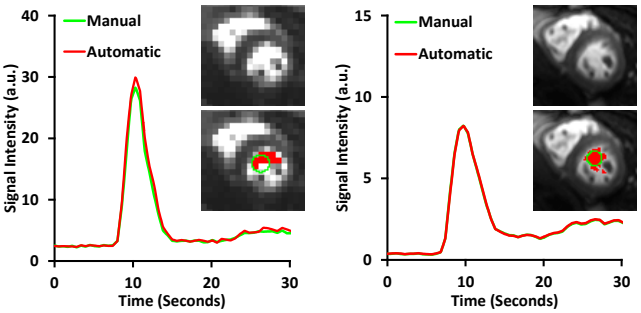

Figure-3. Comparison of the final AIF computed from automatically detected LV pixels vs. manually selected ROI for the examples in Figure-2.

AIF and standard myocardial image series. The temporal statistics of TTP and FWHM showed no significant difference between the two AIF measurements in either low resolution or standard myocardial series. The PV, however, showed significantly higher values for the automated method in both low resolution and standard series ($p<0.01$ and $p<0.001$, respectively). The SI upslope and M-value showed significantly higher values in the automated AIF ($p<0.01$, $p=0.047$) only in the low resolution series; automated results of standard series were still higher, but not significantly (p=NS). These results indicate that the automated method more accurately detected the brightest LV pixels in both image sets, whilst excluding papillary muscle pixels effectively. Both of these are essential to avoid underestimating the AIF peak signal and the upslope measurement. This also highlights the potential subjectivity of manual measurements and the need for consistent and reproducible AIF measurements.

Table-1. Comparison of automated and manual measured AIF. Results are expressed as mean ± standard deviation.

AIF series	Automatic	Manual	p-value
TTP	3.87±1.53	3.77±1.64	NS
FWHM	6.00±2.08	5.78±2.03	NS
PV	41.53±48.8	32.36±37.3	<0.001
Upslope	16.55±23.6	13.16±18.7	<0.01
M-value	2.90±5.24	2.44±4.62	0.047

Myo series	Automatic	Manual	p-value
TTP	4.47±2.40	4.34±1.69	NS
FWHM	7.89±2.94	7.74±2.65	NS
PV	7.93±3.28	7.29±3.08	<0.01
Upslope	2.82±1.56	2.64±1.47	NS
M-value	0.32±0.27	0.30±0.26	NS

For the low resolution AIF series, the execution time averaged 12.29±1.08 seconds for the automated method, while manual methods took 103.04±27.63 seconds. Standard myocardial series averaged 27.62±1.08 seconds for the automated method and 130.87±23.62 seconds for the manual method. The automated method is not only reproducible but also much faster than the manual method.

Out of the 742 image series tested, the automated method successfully measured the AIF from 733 (98.79 %) series. Out of the nine failed series, three were low-resolution AIF series, and six were standard myocardial image series. Of the AIF series, one was due to a failure to detect an atypically shaped RV and in the other two, the signals of the LV and RV were not distinct enough to be accurately separated by the ICA. This is perhaps due to a small heart size, which can introduce large partial-volume errors under such low resolution imaging setting. Five myocardial series failures were due to the incorrect placement of the basal slice during imaging, three toward the LV outflow tract, and two were too far in the opposite direction. Another failure was due to motion artifacts which caused a change in intensity of the background region surrounding the RV, preventing the RV from being correctly detected.

Despite these relatively few failed series, the automated method successfully extracted the AIF for the majority of the series and overcame the main pitfall of manual AIF measurement: papillary muscle exclusion. Papillary muscles, which remain dark throughout the perfusion sequence, can cause underestimation of the AIF if included in the measurement region. In order to avoid these complex structures, an ROI may have to be made very small or irregular in shape which requires more time to draw. The automated method is at an advantage, as it can reliably detect the brightest pixels in the LV blood pool, which can be either connected or discrete regions, to compute an accurate AIF for CMR perfusion quantification.

4. CONCLUSION

We have presented an automated system for measuring the AIF from both standard myocardial and low-resolution AIF CMR perfusion image series. Validation tests have shown it can successfully process a wide array of CMR perfusion images of varying conditions. Automatically measured AIF were found to be in agreement with manual measurements. The automated system has been shown capable of processing a large amount of series, allowing consistently reproducible results, and removing the subjectivity of manual measurement. These improvements may help make quantitative CMR myocardial perfusion analysis more accurate and readily available to assist in the diagnosis of coronary artery disease.

5. REFERENCES

[1] N. Al-Saadi, et al., "Noninvasive detection of myocardial ischemia from perfusion reserve based on cardiovascular magnetic resonance," Circulation, vol. 101, pp. 1379-1383, 2000.

[2] J. Schwitter, et al., "Assessment of myocardial perfusion in coronary artery disease by magnetic resonance: a comparison with positron emission tomography and coronary angiography," Circulation, vol. 103, pp. 2230-2235, 2001.

[3] F.E. Mordini, et al., "Diagnostic accuracy of stress perfusion CMR in comparison with quantitative coronary angiography: fully quantitative, semiquantitative, and qualitative assessment," JACC Cardiovasc Imaging, vol. 7, pp. 14-22, 2014.

[4] M. Jerosch-Herold, "Quantification of myocardial perfusion by cardiovascular magnetic resonance," J Cardiovasc Magn Reson, vol. 12, p. 57, 2010.

[5] L.Y. Hsu, et al., "Automated extraction of the arterial input function from contrast-enhanced first-pass cardiac MR perfusion images," in International Society for Magnetic Resonance in Medicine 19th Annual Meeting & Exhibition, Montreal Canada, p. 3277, 2011.

[6] T.J. Carroll, et al., "Automatic calculation of the arterial input function for cerebral perfusion imaging with MR imaging," Radiology, vol. 227, pp. 593-600, 2003.

[7] D. Peruzzo, et al., "Automatic selection of arterial input function on dynamic contrast-enhanced MR images," Comput Methods Programs Biomed, vol. 104, pp. e148-57, 2011.

[8] J.D. Yin, et al., "Evaluating the feasibility of an agglomerative hierarchy clustering algorithm for the automatic detection of the arterial input function using DSC-MRI," PLOS ONE, vol. 9, 2014.

[9] J. Yin, et al., "Automated detection of the arterial input function using normalized cut clustering to determine cerebral perfusion by dynamic susceptibility contrast-magnetic resonance imaging," J Magn Reson Imaging, doi 10.1002/24642 2014.

[10] P.D. Gatehouse, et al., "Accurate assessment of the arterial input function during high-dose myocardial perfusion cardiovascular magnetic resonance," J Magn Reson Imaging, vol. 20, pp. 39-45, 2004.

[11] V. Gupta, et al., "Cardiac MR perfusion image processing techniques: a survey," Med Image Anal, vol. 16, pp. 767-85, 2012.

[12] M. Benovoy, et al., "Automatic nonrigid motion correction for quantitative first-pass cardiac MR perfusion imaging," to appear in IEEE International Symposium on Biomedical Imaging: From Nano to Macro, 2015.

[13] B. Thomas and M. Jitendra, "Large displacement optical flow: descriptor matching in variational motion estimation," IEEE Trans. Pattern Anal. Mach. Intell, vol. 33, pp. 500-513, 2011.

[14] L.Y. Hsu, et al., "Correcting surface coil intensity inhomogeneity improves quantitative analysis of cardiac magnetic resonance images," in IEEE International Symposium on Biomedical Imaging: From Nano to Macro, pp. 1425-1428, 2008.

[15] P. Comon, "Independent component analysis, a new concept," Signal Processing, vol. 36, pp. 287-314, 1994.